Gridding of Global Precipitation from Asynoptic Satellite Measurements

Murry L. Salby
Program in Atmospheric and Oceanic Sciences
Campus Box 311
University of Colorado
Boulder, CO 80309

February 24, 2003

1. Introduction

Precipitation is observed from space through active and passive microwave techniques. Available from several orbiting platforms, those observations provide continuous global coverage. However, the information content of satellite observations, on which precipitation analysis rests, is limited by the sampling in space and time.

Satellites observe the global precipitation field *asynoptically*: Different sites are observed at different times. Observations are continuous along a satellite's track, but discrete between successive orbits. These features limit the space-time resolution of satellite data. For an individual platform, asynoptic sampling resolves about half a dozen zonal wavenumbers and frequencies less than 1 cpd. The precipitation field, on the other hand, involves variance on much shorter scales.

Variance at short space and time scales is undersampled in satellite data, lying beyond the Nyquist limits of asynoptic sampling. Such variance aliases behavior at longer scales, which would otherwise be correctly represented in asynoptic data. This limitation complicates the gridding of data into synoptic maps of the instantaneous precipitation field. Through the diurnal cycle, undersampled variance also aliases the time-mean precipitation field.

2. Information Content of Asynoptic Data

Rooted in sampling considerations, these errors involve behavior that is misrepresented in asynoptic data. Figure 1 illustrates the sampling along an individual latitude circle from a single platform with about 14 orbits/day. Plotted is the sampling with a Narrow Field of View (NFOV), characteristic of an active instrument like the TRMM radar (solid/open circles). Analogous sampling applies to a Wide Field of View (WFOV), characteristic of a scanning radiometer (shaded). Although capturing instantaneous structure within 25° of longitude, the WFOV likewise leaves most of the precipitation field at that time unobserved.

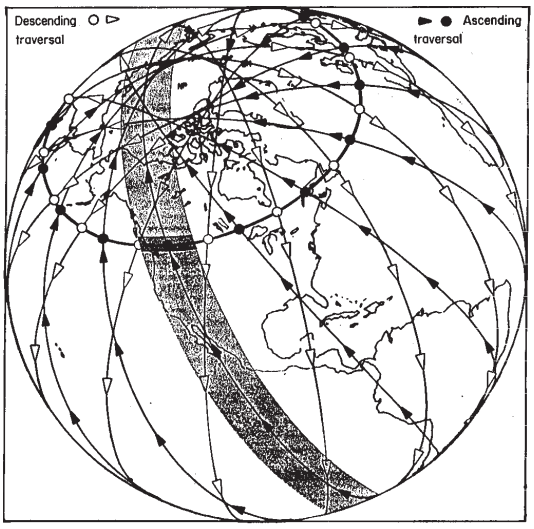

Figure 1: Asynoptic sampling along a latitude circle from a single orbiting platform with a narrow field of view (solid/open circles) and a wide field of view (shading).

For the NFOV, 28 longitudes are observed during one day: 14 from each side of the orbit. Were those longitudes observed simultaneously, this sampling would resolve 14 zonal wavenumbers. On the next day, 28 different longitudes are sampled. They are nested *nonuniformly* within the original 14 longitudes. Collected with those of the first day, they imply the resolution of 28 zonal wavenumbers. After several days, this nested sampling accumulates, yielding a dense mesh of longitudes that, although nonuniform, implies very fine spatial resolution.

The consideration which prevents this benefit is transience. The precipitation field evolves on time scales much shorter than the time for the globe to be covered. Hence, while precipitation is being observed at one site, it is changing at another.

When observations on the latitude circle are represented in extended longitude and time (Fig. 2), the non-uniform character of asynoptic sampling disappears. Observations from the NFOV then form a uniform grid along two "asynoptic coordinates": s and r (Salby, 1982): Each is a mixture of space and time. Much the same picture holds for the WFOV (shaded). Despite high spatial resolution within the instantaneous field of view, the WFOV likewise leaves large gaps in space and time between successive orbits. Small-scale structure within the instantaneous WFOV is incoherent between adjacent orbits (e.g., Lait and Stanford, 1988). Consequently, it does not lend itself to interpolation into a continuous description of the global precipitation field.

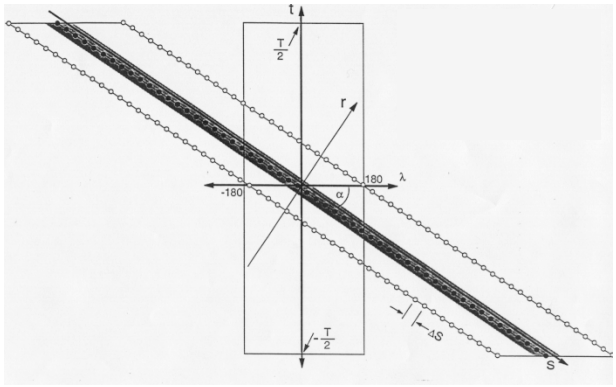

Figure 2: Sampling along the latitude circle, as function of extended longitude λ and time t.

The uniform sampling along asynoptic coordinates establishes the resolution in space and time. It, in turn, defines the information content of satellite data. Illustrated in Fig. 3 in terms of zonal wavenumber and frequency, the information content corresponds to a rectangle oriented along two "asynoptic wavenumbers": k_s and k_r. Analogous to their counterparts in physical space, k_s and k_r are mixtures of synoptic wavenumber and frequency. The boundaries of this rectangle represent the Nyquist limits of asynoptic sampling. Resolved are about 7 zonal wavenumbers and frequencies out to about 1 cpd (0.5 cpd if asymmetry inherent to asynoptic sampling is not accounted for; Salby, 1989). The information content is comparable to that of synoptic sampling, with 14 longitudes observed simultaneously twice per day.

Variance outside this rectangle is undersampled. In the asynoptic data, it is indistinguishable from variance inside the rectangle. An example is illustrated by the two solid circles in Fig. 3: They describe a high-wavenumber stationary component and a low-wavenumber transient component. In a continuous representation along the asynoptic coordinate s (equivalent to time in a reference frame moving with the satellite), those components are mutually distinct (Fig. 4). In the discrete asynoptic data, however, the two components are identical.

Variance outside the Nyquist limits is undersampled. It is therefore misrepresented in the asynoptic data as variance inside the Nyquist limits. Undersampled variance folds back onto behavior at longer (resolvable) scales, which would otherwise be correctly represented.

These sampling considerations are violated by two important classes of variability: (1) Broad-band variance is widely distributed over wavenumber and frequency, spilling beyond the Nyquist limits of asynoptic sampling. (2) Diurnal variations involve harmonics of a day, which lie at and beyond the Nyquist limits. Those harmonics alias zero frequency, introducing a bias into the time-mean distribution. These classes of variability challenge the information content of asynoptic data. They also represent the two major elements of the precipitation field.

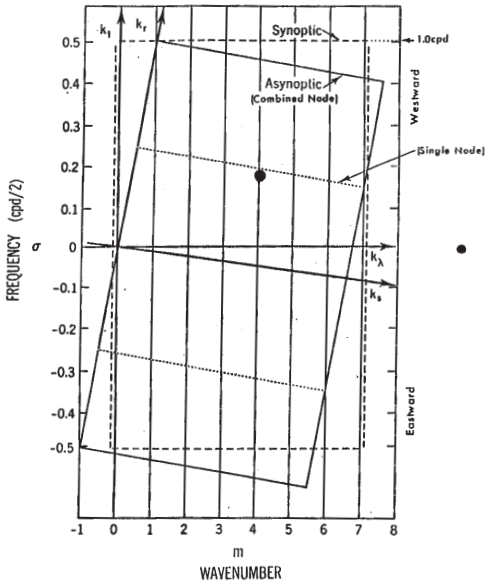

Figure 3: Information Content of asynoptic data from a single platform, as function of zonal wavenumber k_λ and frequency k_t.

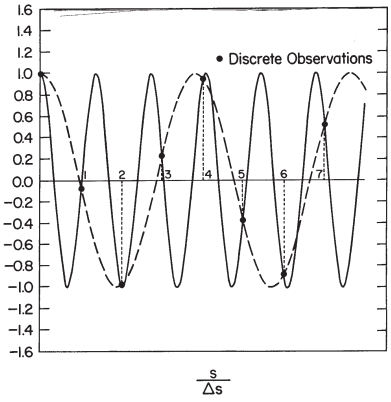

Figure 4: Behavior along asynoptic coordinate s of a high-wavenumber stationary component and a low-wavenumber transient component (solid circles in Fig. 3), which form an alias pair. Values actually sampled by satellite indicated in solid circles.

3. High-Resolution Description of Convection

The impact of undersampled variance has been studied in high-resolution Global Cloud Imagery (GCI), which has been constructed from 6 satellites simultaneously monitoring the earth (Salby et al., 1991). Illustrated in Fig. 5, each image represents a nearly instantaneous snapshot of the global convective pattern. With horizontal resolution of 0.5° and temporal resolution of 3 hrs, the GCI resolves the dominant scales of organized convection.

Cold cloud fraction η_c provides a proxy for areal-averaged rainfall (e.g., Richards and Arkin, 1981), serving as a cornerstone even in diverse analyses like GPCP that include ground-based measurements (Huffman et al., 1997). Through η_c, the GCI has been married with monthly-mean precipitation in GPCP to map the global distribution of rainfall at horizontal resolution of 2.5° and temporal resolution of 3 hrs. In the sampling experiments below, we rely on the raw imagery of η_c in the GCI. Available at increments of 0.5° and 3 hrs, it provides short-scale behavior that approaches the granularity of the actual precipitation field. The GCI then provides a litmus test of asynoptic sampling.

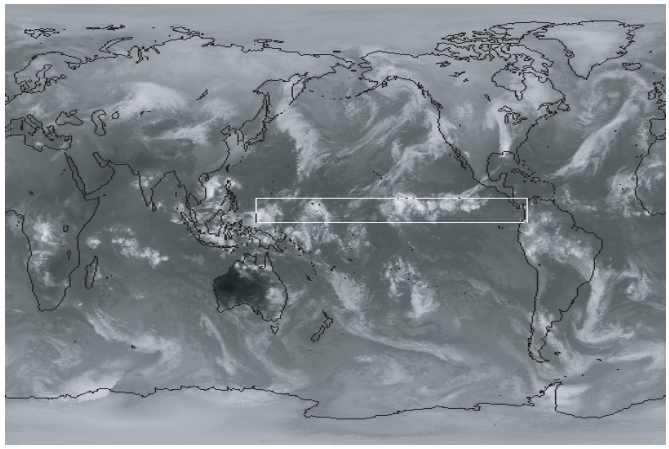

Figure 5: Global Cloud Image (brightness temperature) at 06Z on Nov 17, 1987.

Figure 6 plots the frequency spectrum of cold cloud, over tropical Africa. The spectrum at individual sites (dotted) is broad band, punctuated by pronounced spikes at harmonics of the diurnal cycle. Those harmonics reflect brief but heavy rainfall at preferred local times, which contributes disproportionately to the daily accumulation (Janowiak et al., 1994). More sobering is what happens if cold cloud is averaged spatially over the convective center. The spectrum (solid) is then dominated by diurnal variance. Unlike other fluctuations, the diurnal variation is spatially coherent across the region of convection (Bergman, 1996; Bergman and Salby, 1996). Consequently, it is not removed by spatial averaging. It is, in fact, the large-scale coherent component that is important for climate studies and for refining models.

4. Aliasing by the Diurnal Cycle

We turn now to what undersampled variance implies for deriving the time-mean distribution. To cope with diurnal variance, satellites are flown in a precessing orbit: Observations on a latitude circle then drift through local time, eventually sampling all phases of the diurnal cycle. However, even this sampling is limited by two practical considerations: (1) The precession period is long, typically a month or longer. (2) The diurnal variation is not steady, but random. It varies from one day to the next according to the presence of convection. These considerations require *a population of observations*, several at each local time, to composite the mean diurnal variation. Only in a large enough population is the mean diurnal variation truly separated from the time mean.

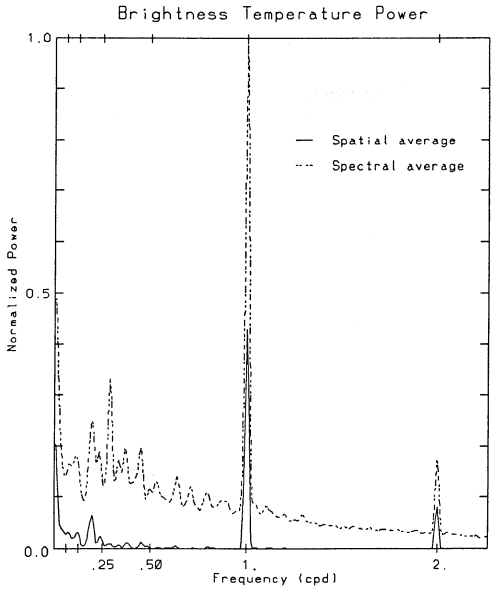

Figure 6: Frequency spectrum of cloud over tropical Africa: Ensemble average of spectra at individual 0.5° locations (dashed) vs spectrum of areal average (solid).

To evaluate the systematic error from diurnal aliasing, the GCI has been sampled asynoptically from a single platform with specified orbital and viewing geometries. The resulting time-mean distribution is then compared against the true time mean in the GCI. Figure 7 plots the relative error recovered from a WFOV, with a precession period of about a month. After 1 month of averaging, the bias from undersampled diurnal variance exceeds 50% over regions of tropical convection. Even after 3 months of averaging (not shown), the systematic error still exceeds 30%.

Figure 8 plots the same information, but for a NFOV. The systematic error is noticeably greater. After 1 month of averaging, it approaches 80% in regions of tropical convection. Even after 3 months of averaging (not shown), the bias exceeds 40%.

The different systematic errors produced by these viewing geometries follows from how often individual sites are sampled (Salby and Callaghan, 1997). During one month, a 2.5° cell is sampled by the NFOV instrument 50–100 times. This yields only 2–4 observations per hour of local time for each 2.5° cell. In contrast, the same cell is sampled by the WFOV instrument an order of magnitude more frequently. The larger population better separates the mean diurnal variation from the time mean, which then contains a smaller bias.

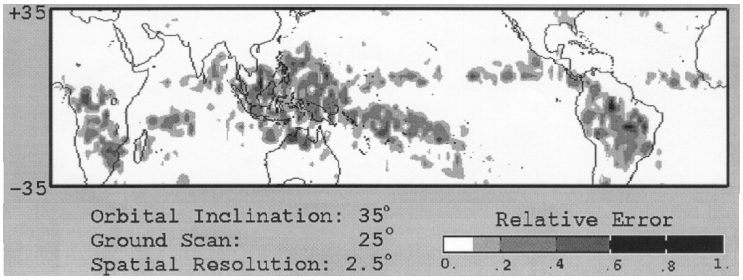

Figure 7: Relative bias from diurnal aliasing after averaging asynoptic observations over 1 month. Derived from a precessing orbit with a WFOV (25° ground scan).

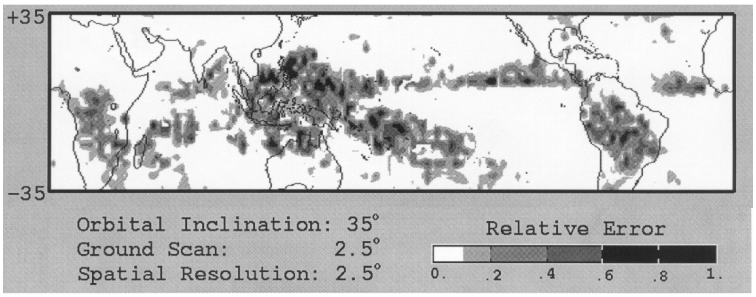

Figure 8: As in Fig. 7, but for a NFOV (2.5° ground scan).

5. Synoptic Mapping of Large-Scale Structure

We turn next to undersampled small-scale variance and its implications for synoptic maps of global structure. Constructing synoptic maps is more ambitious than the time-mean distribution. However, two features work in its favor: (1) Small undersampled scales are not of primary interest in climate applications. Rather, it is their organization by large scales that is most important. (2) Aliases of those undersampled scales are random.

A technique has been developed to reject undersampled incoherent variance, leaving a more accurate representation of large-scale coherent variance (Salby and Sassi, 2001), As before, the GCI is sampled asynoptically from a single orbiting platform. Figure 9a plots, from the raw sampled data, the spectrum over asynoptic wavenumber k_s. (It is equivalent to the spectrum over frequency in a frame moving with the satellite.) Broadly distributed over wavenumber, the spectrum is statistically white. It can be shown that only variance within a neighborhood of integer k_s lies within the asynoptic rectangle of Fig. 3. Variance removed from integer k_s, which dominates the spectrum in Fig. 9a, is then undersampled. Figure 9b plots the same information, but after the technique has been applied to the raw asynoptic data. Variance is now concentrated about integer k_s. Variability has therefore been discriminated to those space and time scales that are resolved in the asynoptic data.

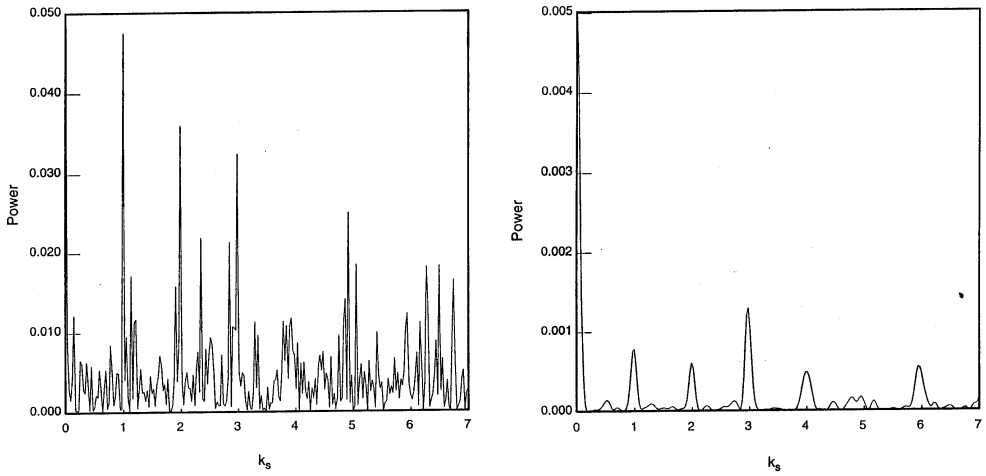

Figure 9: Power spectrum of cold cloud, as function of asynoptic wavenumber k_s, (a) from raw asynoptic data and (b) after processing to reject incoherent variance.

This technique has been applied to data sampled asynoptically from the GCI to produce daily synoptic maps over a 1-month period. The results are then compared against the true synoptic behavior in the GCI. When synoptic maps are produced from the raw asynoptic data, the error at large scales is as great as the large-scale signal present. However, when the asynoptic data are processed via this technique, the error variance is reduced to 10% or less.

Figure 10 illustrates the synoptically-mapped evolution over the equatorial central Pacific. The period shown includes an amplification of the Madden-Julian oscillation (MJO), which organizes tropical convection. In the synoptically-mapped evolution (dashed), cold cloud is magnified during the first week, when convection in the MJO crosses the dateline. Cold cloud then decreases sharply, as convection migrates eastward and leaves the region. The mapped evolution faithfully tracks the true large-scale evolution in the GCI (solid). So does the global structure in synoptic maps (ibid.).

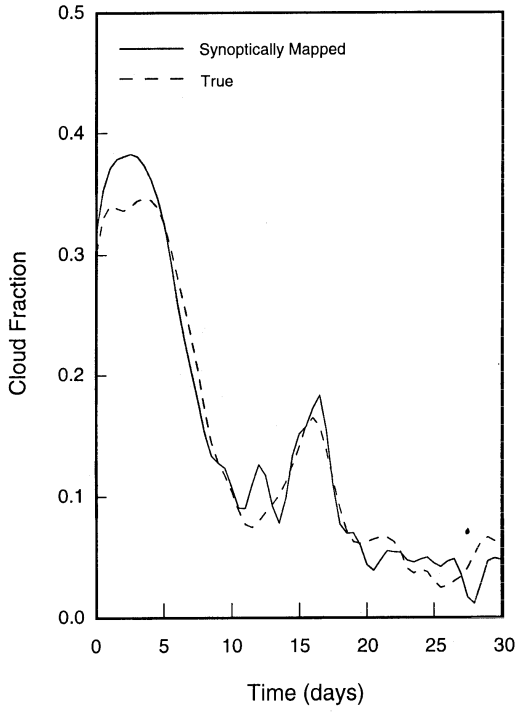

Figure 10: Large-scale evolution of cold cloud over central Pacific (a) in synoptically-mapped behavior and (b) actually present in GCI.

6. Representation of Convection in Models

Analyzed precipitation, derived through a model, must contend with the misrepresentation of scales in asynoptic data. A precipitation analysis also relies on the model's representation of precipitation. It competes with observed precipitation where measurements are available, but serves in place of them where they are not.

In general, cumulus convection is poorly represented in models, as is its diurnal variation. Although details of its simulation vary with model and convective parameterization, certain forms of pathological behavior are common to many GCMs. Figure 11 plots, from the BMRC model, the forecast distribution of cloud brightness temperature for the same time as in Fig. 5. Comparison shows that the model reproduces observed structure remarkably well at middle and high latitudes, where cloud is organized by sloping convection. In the tropics, however, where cloud is organized by cumulus convection, the simulation is less successful. Not only does the instantaneous structure differ, but so does the evolution.

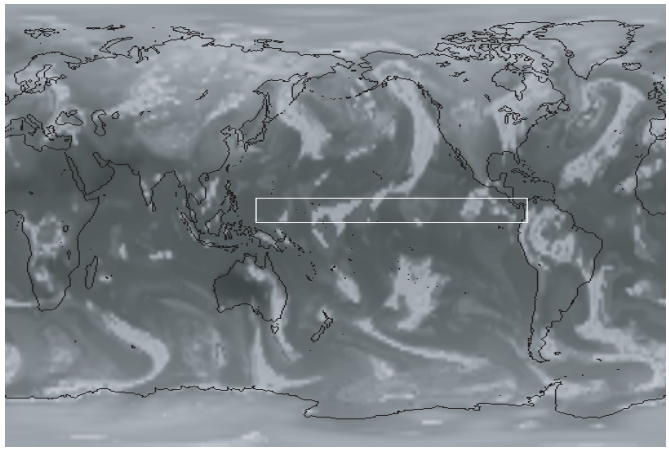

Figure 11: As in Fig. 5, but simulated in a 2-day forecast by the BMRC model.

The simulation in the tropics deviates from observed behavior on the time scale of days and, most conspicuously, in relation to the diurnal cycle. This form of pathological behavior is not unique to the BMRC model. In fact, it is intrinsic to many GCMs, including the COLA model and the NCAR CCM (Ricciardulli and Garcia, 2000). Figure 12 compares the power spectrum of areal-averaged precipitation over the equatorial Pacific (inside the window shown in Figs. 5 and 11) represented in the GCI vs that simulated during the same period by the COLA model. The observed behavior (Fig. 12a) involves a red spectrum, in which variance is distributed broadly out to 1 cpd. The diurnal cycle, although present, is comparatively minor because the region considered is principally maritime. In the simulated behavior (Fig. 12b), however, power is sharply concentrated at low frequency and at the diurnal cycle. At intermediate scales, where convection is organized through interaction with the circulation, power is virtually absent. Analogous behavior is evident in other models (ibid.). Depending on the convective parameterization, the diurnal cycle can be even stronger, dominating the organization of tropical convection.

7. Implications

Aliasing by undersampled diurnal variance is significant over much of the tropics. This is especially true near land, where convection undergoes a pronounced diurnal variation. The time-mean precipitation field can therefore be determined only as accurately as can the mean diurnal variation. This systematic error requires data from a single platform to be averaged over several months – even if that platform is in a precessing orbit.

The random component of sampling error can be sharply reduced by rejecting incoherent variance. Large-scale coherent structure, describing the organization of precipitation, can then be mapped synoptically on individual days. This opens the door to a wide range of scientific applications, including issues surrounding how precipitation interacts with the general circulation.

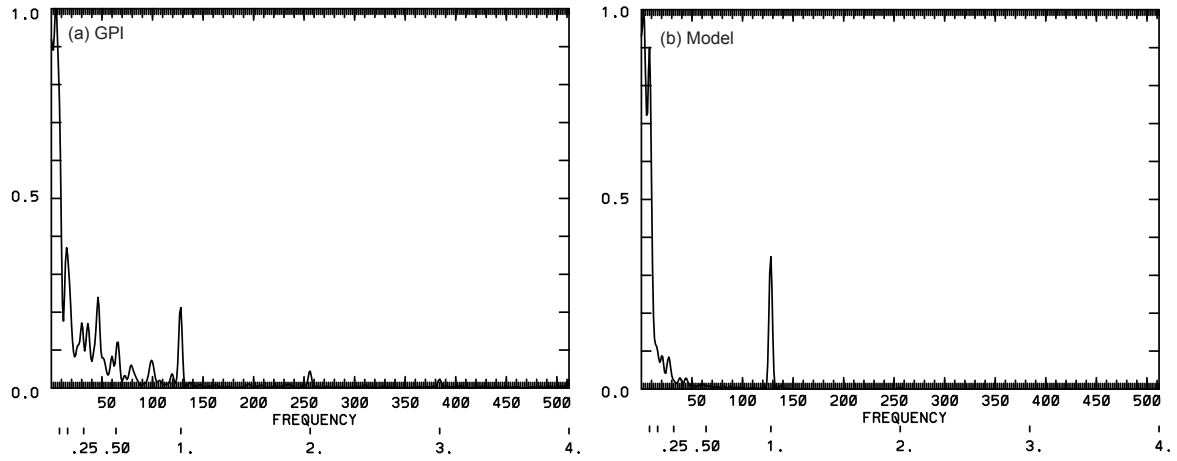

Figure 12: Power spectra of areal-averaged precipitation over equatorial Pacific, indicated in Fig. 5, (a) represented in the GCI and (b) simulated by the COLA model.

The foregoing limitations stem from sampling error, which leads to a misrepresentation of scales in asynoptic data. Once the precipitation field has been undersampled, aliased behavior is difficult to distinguish from behavior that is genuinely present. This feature is an important consideration for assimilating satellite measurements into a forecast model. Beyond incorporating observed behavior, the model generates precipitation at other locations and times, for which observations are absent. The characteristic scales of precipitation are much shorter than space-time gaps in asynoptic data from a single platform. For this reason, only the large-scale organization and statistics of observed precipitation can be interpolated reliably into a continuous description of the global precipitation field. An accurate analysis of global precipitation will require (1) the input data to be properly interpreted and (2) statistical properties and the organization of precipitation in the model, inclusive of the diurnal cycle, to faithfully represent counterpart behavior in the atmosphere.

The ultimate solution to these limitations is more frequent sampling in space and time. This feature is provided by *multiple orbiting platforms*. If details of the combined sampling are accounted for, such precipitation measurements make possible accurate monthly-mean structure, as well as synoptic maps with enhanced frequency and horizontal resolution.

References

Bergman, J. and M. Salby, 1996: Diurnal variations of cloud cover and their relationship to climatological conditions. *J. Climate* **9**, 2802-2820.

Bergman, J., 1996: A numerical investigation of cloud diurnal variations. *J. Climate* **10**, 2330-2350.

Huffman, G., Adler, R., Arkin, P., Chaing, A., Ferraro, R., Gruber, A., Janowiak, J., McNab, A., Rudolf, B., and U. Schneider, 1997: The Global Precipitation Climatology Project (GPCP) combined precipitation data set. *Bull. Amer. Meteorol. Soc.*, **78**, 5–20.

Janowiak, J., Arkin, P., and M. Morrissey, 1994: An examination of the diurnal cycle in oceanic tropical rainfall using satellite and in situ data. *Mon. Wea. Rev.*, **122**, 2296-2311.

Lait, L. and J. Stanford, 1988: Applications of asynoptic space-time Fourier transform methods to scanning satellite measurements. *J. Atmos. Sci.*, **45**, 3784-3799.

Ricciardiulli, and R. R. Garcia, 2000: The excitation of equatorial waves by deep convection in the NCAR community climate model (CCM3) *J. Atmos. Sci.*, **57**, 3461-3487.

Richards, F., and P. Arkin, 1981: On the relationship between satellite-observed cloud cover and precipitation, *Mon. Wea. Rev.*, **109**, 1081–1093.

Salby, M. L., 1982: Sampling theory for asynoptic satellite observations *J. Atm. Sci.*, **39**, 2577–2600.

Salby, M., 1989: Climate monitoring from space: Asynoptic sampling considerations. *J. Climate*, **2**, 1091-1105.

Salby, M. L., H. Hendon, K. Woodberry, and K. Tanaka, 1991: Analysis of global cloud imagery from multiple satellites. *Bull. Am. Meteorol. Soc.*, **72**, 467–480.

Salby, M. and P. Callaghan, 1997: Sampling error in climate properties derived from satellite measurements: Consequences of undersampled diurnal variability. *J. Climate*, **10** 18-36.

Salby, M. and F. Sassi, 2001: Synoptic mapping of convective structure from undersampled satellite observations. *J. Climate*, 15, 2281-2295.